# Development of Flow over Blunt-Nosed Slender Bodies at Transonic Mach Numbers

# Development of Flow over Blunt-Nosed Slender Bodies at Transonic Mach Numbers

**Gireesh Yanamashetti[1†], G. K. Suryanarayana[2†] and Rinku Mukherjee[3]**

[1]PhD Scholar & Senior Scientist, [2]Chief Scientist, [3]Assistant Professor
[†]National Aerospace Laboratories, Bangalore, India 560017
[3]Dept.of Applied Mechanics, Indian Institute of Technology Madras, India 600036

E-mail: [1]gireesh@nal.res.in, [2]surya@nal.res.in, [3]rinku@iitm.ac.in

**Abstract.** Comparisons of the development of flow over a cylinder with a $20^o$ cone nose and a cylinder with an ogive nose, which represent typical heat-shield configurations are studied using CFD and experiments at transonic Mach numbers. The $C_p$ plots are studied to locate expansion or separation. Experiments are carried out at $M = 0.8$, 0.9, 0.95 and 1.1 and $Re \approx 2.45 \times 10^6$. Computations are carried out using the commercial package, FLUENT 6.3. Inadequate spatial resolution of pressure ports in experiments as well as limitations of the CFD tool result in some differences in experimental and CFD results.

## 1. Introduction

It is well known that transonic flows are extremely complicated to comprehend because of the mixed nature of the flow involving local pockets of subsonic and supersonic flows. For slender bodies such as launch vehicles, rockets, missiles etc., the payload is placed around the nose, i.e. around the region of the heat shield. Hence, proper understanding of the flow features around the nose is extremely important for successful accomplishment of the mission. Considering geometry of the main rocket engine, volume of the payload and the specific requirements of a mission, use of conical nose shapes along with boat tail [1] are often needed. During the flow, the external structure of the heat shield is subjected to steady as well as unsteady pressure loading [2]. Frequency contents in the external flow can excite the structural modes and result in undesirable levels of vibrations of components mounted inside the heat shield [3].

Since boundary layer separation and reattachments are sources of noise and unsteady forcing of the structure, such features should be avoided in the design of the heat shield. With significant advances made in CFD, it is desirable to exploit the capabilities of CFD tools to obtain deeper understanding of complex transonic flows after validation with experimental data. Hence, in this paper the transonic flow features of two heat-shield configurations, which have nearly identical volume and boat-tail angles but with different nose shapes are compared based on experiments and computations.

## 2. Experimental Set-Up

The 1.2m Trisonic Wind Tunnel at CSIR-NAL is an intermittent blowdown facility providing maximum run duration of about 40 sec. operating from storage receivers at maximum pressure

of 150 psig. The Mach number capability is from 0.2 to 4.0. Subsonic Mach numbers in the test section are achieved by choking the second throat. Supersonic speeds are achieved by variation of nozzle contour using a flexible nozzle Transonic Mach numbers are achieved using a transonic insert with a perforated wall test section. The top and bottom walls of the insert have 0.5 inch diameter inclined holes with 6% open area ratio, the sidewalls have normal holes with an open area ratio of 20%. Acoustic baffles are used in the plenum chamber of the transonic insert to reduce flow unsteadiness in the test section. Test Reynolds number within a certain range can be achieved by variation of the tunnel stagnation pressure. The model incidence may be varied from$15^o$ to $27^o$ continuously or in steps during a run and the model can be rolled and locked from $0^o$ to $360^o$ prior to a run.

*2.1. Models used and Test Conditions*

The model with a $20^o$ nose consists of a hemispherical nose matched to a $20^o$ cone, cylindrical region and a $20^o$ boat-tail followed by a cylindrical region. The model with an ogive nose is nearly identical, except for the total length, which is greater by $0.16d$ as shown in Fig. 1. Details of the geometry of the models are shown in Fig. 2.

Experiments are carried out at $M = 0.8$, 0.9, 0.95 and 1.1 and a Reynolds number based on the maximum diameter, $Re \approx 2.45 \times 10^6$. Boundary layer trip was located at 5% of the length of the nose on both the models. The pitch angle was fixed at $0^o$ to ensure axisymmetric flow.

*2.2. Model Instrumentation*

The models have pressure ports along different generators. Pressure data from the $0^o$ generator and at AOA = $0^o$ alone are discussed here for the purpose of validation of the computations. Surface pressure measurements were carried out using electronically scanned pressure (ESP) scanners (32 ports/16 ports) of range 15 psid housed inside the model. The total tunnel pressure and static pressures were measured in the settling chamber and plenum chamber respectively using 150 psia and 15 psid pressure transducers. All the pressure data from the ESP scanners were acquired at each angle of attack after an initial dwell of 1.2 seconds. At each port, the channels were scanned at the rate of 500 samples per second and a total of 20 samples per channel were acquired at each angle. The averaged pressure data are presented in this paper. Uncertainty in pressure is 0.0045 psi, within 0.1% of range of pressure transducers/scanner employed. Mach number repeatability is within 0.005.

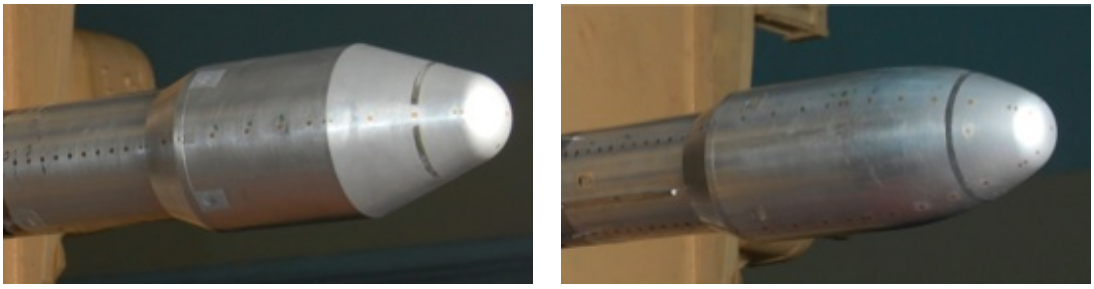

(a) Model with $20^o$ cone nose (b) Model with ogive nose

Figure 1: Models

## 3. Numerical Simulation

Axisymmetric analysis was carried out using Euler equations using the commercial software package FLUENT 6.3. For the study $Re = 2.45 \times 10^6$, based on the maximum diameter.

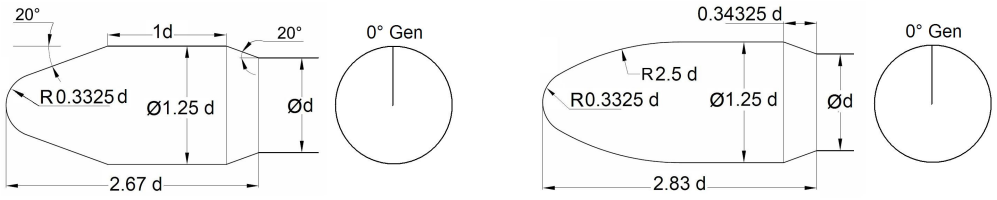


(a) Model with $20^o$ cone nose (b) Model with ogive nose

Figure 2: Details of Geometry of Test Models

Ansys Gambit was used for grid generation and Ansys FLUENT for solving the governing Euler equations. Mass conservation equation is the same as for a laminar flow but the momentum and energy conservation equations are reduced due to the absence of molecular diffusion. For 2D and axisymmetric bodies, the continuity equation as given in Eqn. 1. Axial and radial momentum conservation equations are given in Equations 2 and 3 respectively. The equation for conservation of energy is given in Eqn. 4.

$$\frac{\partial \rho}{\partial t} + \frac{\partial}{\partial x}(\rho v_x) + \frac{\partial}{\partial r}(\rho v_r) + \frac{\rho v_r}{r} = S_m \tag{1}$$

$$\frac{\partial}{\partial t}(\rho v_x) + \frac{1}{r}\frac{\partial}{\partial x}(r\rho v_x v_x) + \frac{1}{r}\frac{\partial}{\partial r}(r\rho v_r v_x) = -\frac{\partial p}{\partial x} + F_x \tag{2}$$

$$\frac{\partial}{\partial t}(\rho v_r) + \frac{1}{r}\frac{\partial}{\partial x}(r\rho v_x v_r) + \frac{1}{r}\frac{\partial}{\partial r}(r\rho v_r v_r) = -\frac{\partial p}{\partial r} + F_r \tag{3}$$

$$\frac{\partial}{\partial t}(\rho E) + \nabla \cdot (\vec{v}\,(\rho E + p)) = -\nabla \cdot \left(\sum_j h_j J_j\right) + S_h \tag{4}$$

The computational domain is shown in Fig. 3. The flow is simulated as in the wind tunnel i.e. the top boundary is defined as wall. A structured grid was generated using Ansys Gambit. The present computations were carried out on $470 \times 175$ grids. Successive ratios of 1.016 to 1.06 are used depending on regions requiring finer mesh. Standard settings of inviscid model of Fluent are applied. First order upwind, implicit time marching schemes were used. The residuals were converged to $10^{-5}$. The net mass flow rate balanced till 0.05 Kg/s.

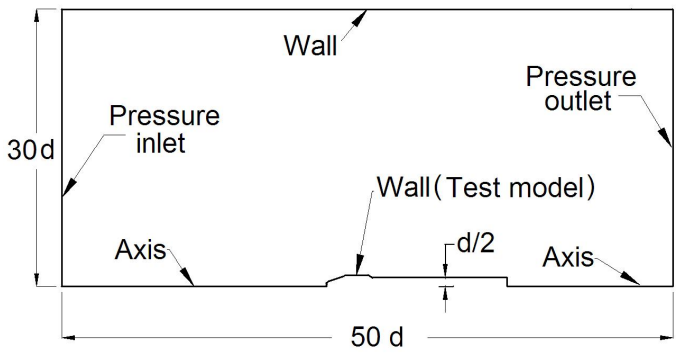


Figure 3: Computational Domain and Boundary Conditions

## 4. Results

Figure 4 shows a comparison of the experimental and computed $C_P$ distributions on both the models at 4 different Mach numbers, which are in the transonic range. The blue and red dotted lines are model geometry profiles of $20^o$ nose and Ogive nose models respectively. Rapid expansion of the flow as shown by the sharp drop in $C_p$, starting from the stagnation point ($C_p = 1$) is noted for all Mach numbers. The front of the model is a region of favourable pressure gradient. However, a short separation bubble of length, $x/d \approx 0.1$ exists, which is shown by the static $C_p$ curve at the junction where sphere and cone meet, i.e. at $x/d \approx 0.3$. This may be attributed to the sudden change in curvature although the local slope is continuous. This has also been reported in literature [4]. Stronger expansion of the flow around the shoulder region ($x/d \approx 1.0$) is observed for the conical nose compared to the ogive nose.

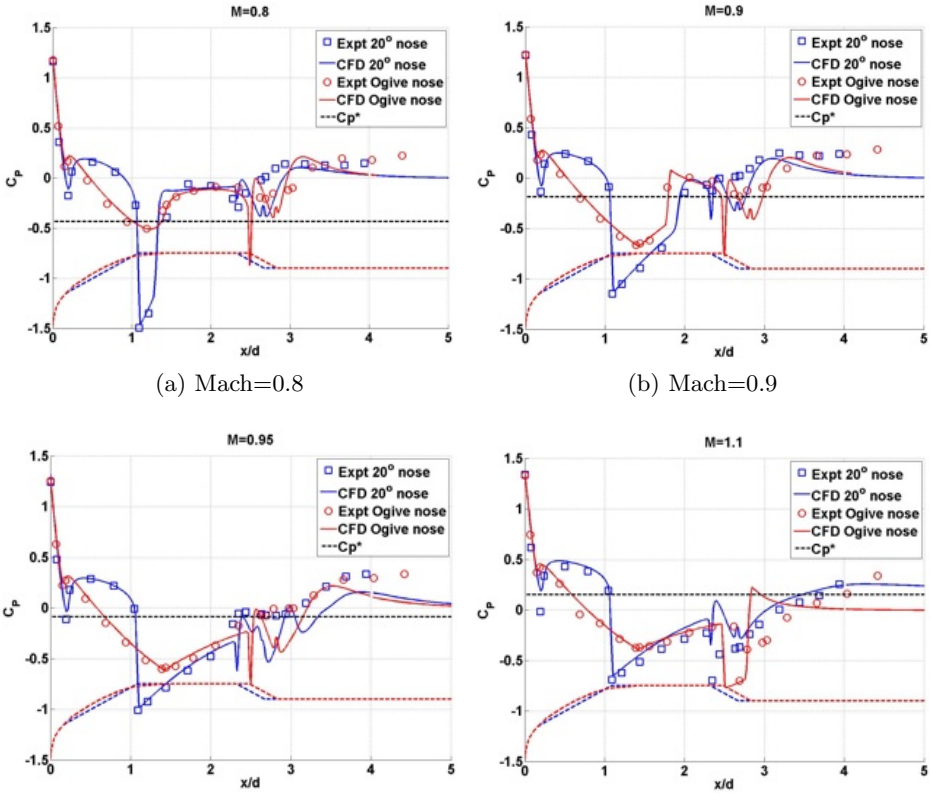


(a) Mach=0.8 (b) Mach=0.9

(c) Mach=0.95 (d) Mach=1.1

Figure 4: Static Pressure Distributions

As shown in Fig. 4a, for the $20^o$ nose, the $C_p$ drops to a minimum of -1.5 while for the ogive cone it is $\approx -0.5$. The $C_p$ minima for the ogive cone is also further downstream of $x/d \approx 1.0$. With increase in Mach number as shown in Figures 4b to 4d, the $C_p$ minima for the $20^o$ nose increases, continuing to be located at $x/d \approx 1.0$ while that for the ogive cone decreases and its distance from $x/d \approx 1.0$ also increases. At Mach=0.8 and 0.9, as shown in Figures 4a and 4b, the $C_p$ minima is followed by a shock over the $20^o$ nose whereas there is no shock over the ogive cone. Consequently, shock induced separation occurs on the conical nose as indicated by the pressure plateau in experiments as well as in computations.

Around the boat-tail of the conical nose, computations indicate expansion (drop in $C_p$) followed by a shock whereas experiments indicate subsonic flow (+ve $C_p$). This is due to the

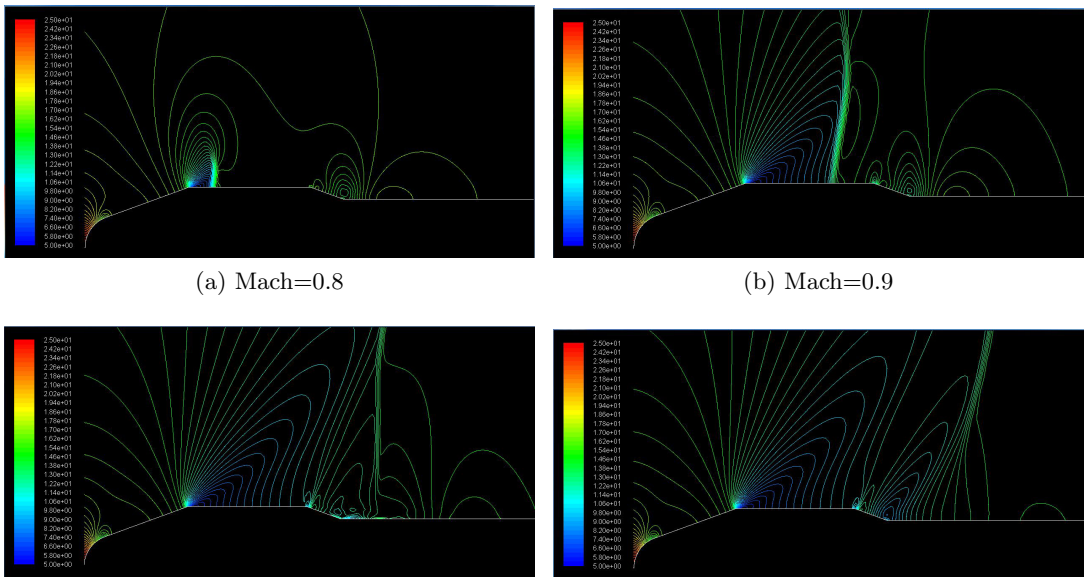

(a) Mach=0.8 (b) Mach=0.9

(c) Mach=0.95 (d) Mach=1.1

Figure 5: Shock Movement on nose with $20^o$ cone

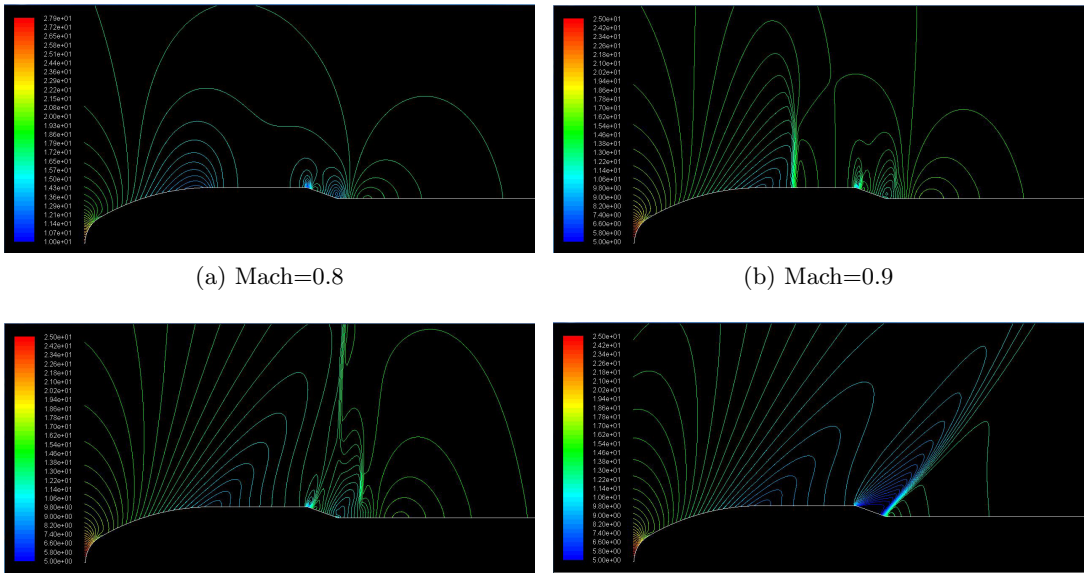

(a) Mach=0.8 (b) Mach=0.9

(c) Mach=0.95 (d) Mach=1.1

Figure 6: Shock Movement on nose with ogive cone

inadequacies in the spatial resolution of pressure ports in experiments as well as in the CFD tools used here, which do not enable a fair comparison. Around the boat-tail of the ogive nose, though both computations and experiments indicate subsonic flow but the agreement in $C_p$ values is not satisfactory. Ambient conditions ($V = V_\infty$, $C_p = 0$) are reached in computation around $x/d \approx 4.0$ whereas in experiments, free-stream conditions are not reached even at $x/d = 4.4$.

The location of the normal shock at these Mach numbers for the $20^o$ nose and the ogive cone is shown in Figures 5 and 6 respectively. The colour key shows bottom most blue for 5

psi and top most red for 25 psi pressure.The comparison of the movement of the shock on both the models is shown in Fig. 7. The normal shock moves downstream as the Mach number is increased, as expected for any configuration. Occurrence of shock is delayed on the conical nose as compared to ogive nose in the transonic range, suggesting that the critical Mach number for the ogive nose cone is higher.

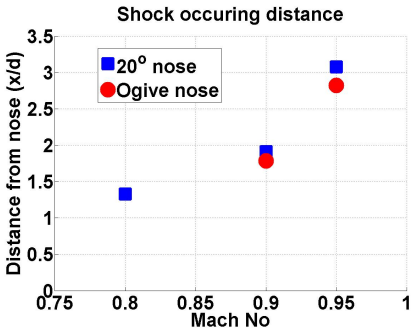


Figure 7: Location of the Normal Shock at different Mach Numbers

## 5. Conclusion

Comparisons between experiments and computations at transonic Mach numbers on conical and ogive nose-shaped slender bodies with boat-tails is good towards the upstream side. Comparison is not good along the boat-tail, separated flow regions and downstream of the boat-tail for axisymmetric flow conditions. Expansion of the flow around the shoulder region for the conical nose is stronger compared to the ogive nose. Around the boat-tail, both computation and experiment indicate subsonic flow but the agreement in $C_p$ values is not satisfactory. Occurrence of shock is delayed on the ogive nose compared to conical nose. Flow over the ogive nose cone is smoother with much reduced pressure gradients along the body compared to the conical nose. Hence, it seems that the transonic flow over the ogive nose is less prone to flow separation as compared to that over the $20^o$ conical nose.

***Acknowledgement***

Authors would like to acknowledge the Director, CSIR-National Aerospace Laboratories for grant of the internal research project (N-8-503), which enabled the present study. Support provided by the staff of Design Section, NTAF, Model Shop and 1.2m tunnel is acknowledged. Special thanks to Mr. T. Arun Kumar, Scientist, NTAF for assistance in wind tunnel tests.

## References

[1] Charles F. Coe, Steady and fluctuating pressures at transonic speeds on two space vehicle payload shapes, NASA TM X-503, March 1961.
[2] Lawrence, A.G, Gary, A. A., Gallis, M. A. Jr. and George S Deiwert, Comparison of computations and experiments for non-equilibrium flow expansions around blunted cone, AIAA 96-0231, 1996.
[3] R. C. Mehta, Unsteady flow field characteristics over blunt bodies at high speeds, http://dx.doi.org/10.5772/57050, chapter 5, Intech, 2014.
[4] M. A. Ramaswamy and G. Rajendra, Experimental investigation of transonic flow past blunt cone cylinder, Journal of Spacecraft and Rockets, Vol.15, No.2,1978, pp. 120-123. doi: 10.2514/3.28001